Effects of Graphene Oxide on Tribological Properties of Micro-Arc Oxidation Coatings on Ti-6Al-4V

Qingyuan Hu , Xingming Li , Gai Zhao * , Yuling Ruan , Guoqing Wang , Qingjun Ding

Posted Date: 20 October 2023

doi: 10.20944/preprints202310.1334.v1

Keywords: Micro-arc oxidation; Ti-6Al-4V titanium alloy; graphene oxide; friction and wear

Article

Effects of Graphene Oxide on Tribological Properties of Micro-Arc Oxidation Coatings on Ti-6Al-4V

Qingyuan Hu, Xingming Li, Gai Zhao *, Yuling Ruan, Guoqing Wang and Qingjun Ding

State Key Laboratory of Mechanics and Control of Mechanical Structures, Nanjing University of Aeronautics and Astronautics, Nanjing 210016, China

* Correspondence: zhaogai@nuaa.edu.cn; Fax: +86 25 84896131

Abstract: Micro-arc oxidation (MAO) is an emerging technology employed to produce high hardness or anti-corrosion ceramic coatings on lightweight metals such Al, Ti, Mg and their respective alloys. However, under non-lubrication conditions, such coatings exhibit relatively high friction coefficients. To enhance the friction reduction properties of the MAO coatings, we employed a one-step MAO process with varying concentrations of graphene oxide (GO) in an aluminate system electrolyte to create composite coatings on the surfaces of Ti-6Al-4V alloy. The effect of concentrations of GO particles on microstructure, composition, and wear behavior of the resulting composite coatings was investigated. Measurements of the coating's thickness, hardness, and roughness have also been conducted. Ball-on-disk friction test under dry condition were carried out to reveal tribological behavior of the MAO coating. The addition of graphene oxide in the electrolyte reduces the friction coefficient, with the composite coating containing 5 g/L of GO particles displaying the most effective friction reduction. Moreover, coating thickness increases with higher GO concentration. This friction reduction can be attributed to the particles in the coating acting as lubricants during friction, while GO also reduces adhesive damage, shifting the wear mechanism from adhesive to abrasive.

Keywords: Micro-arc oxidation; Ti-6Al-4V titanium alloy; graphene oxide; friction and wear

1. Introduction

Owing to its high strength-to-weight ratio, excellent corrosion resistance and biocompatibility, titanium alloy have been extensively used in aerospace, marine and biomedical industries[1]. The TC4 titanium alloy is currently the most widely used α+β titanium alloy, its amount accounts for more than half of the total consumption of titanium alloys[2]. Components made from titanium alloys are often in tribological contact with different media, under stationary or dynamic loading[1]. And the poor tribological properties of titanium alloy, such as low surface hardness, high friction coefficient, and poor wear resistance, have limited their scope of application[3]. Some surface engineering techniques that have been employed for titanium alloy include surface oxidation, PVD/CVD coating, ion implantation etc[4]. However, these methods are quite expensive and may not provide a thick layer. As the most popular technique for the surface modification of titanium alloy, anodic oxidation generates thin films of amorphous hydrated oxide or crystalline TiO_2 in the anatase form, which can't provide adequate load support under heavy load[5,6].

Micro-arc oxidation (MAO), also referred as plasma electrolytic oxidation (PEO), is an environmentally friendly technology used to produce ceramic coatings with good adhesion on valve metals such as aluminum (Al), titanium (Ti), magnesium (Mg), zirconium (Zr), and their alloys[7]. This technique is similar to metal anodic oxidation within an electrolytic solution, employing voltages that induce plasma micro-discharges at the electrode's surface. This film is modified through spark micro-discharges initiated at potentials exceeding the breakdown voltage of the growing oxide film and rapidly moving across the anode surface[8]. At the same time, the local temperature and pressure within the discharge channel can reach 10^3-10^4 Kelvin and 10^2-10^3 MPa[9]. These conditions are high enough to induce plasma thermochemical interactions between the substrate and the electrolyte[10]. These interactions result in the formation of melt-quenched high-temperature oxides and complex compounds on the surface. These compounds consist of oxides of both the substrate material and

 doi:10.20944/preprints202310.1334.v1

modifying elements carried by the electrolyte[11]. These coatings typically have high wear resistance due to its high hardness, but exhibit high friction under dry friction condition[12]. The property and quality of the ceramic coatings can be adjusted by changing the composition of the electrolyte, various electrical parameters and the process temperature[13].

Researchers have attempted to reduce the friction coefficient and enhance wear resistance of the coatings by synthesizing self-lubricating coatings through a one-step process in lubricant-containing solutions[14]. Chang et al.[15] reported that good adhesion and better tribological properties were obtained for the MAO grown coatings by adding 4 g/L MoS_2 particles in the electrolyte. Liu et al.[16] prepared a composite coating containing graphene nanosheets and TiO_2 on Ti-6Al-4V alloy. The addition of graphene provides higher hardness and smoother surface, resulting in improved wear resistance. Zhang and coworkers[17] investigated the influence of Graphene oxide (GO) on tribological and corrosion performance of magnesium alloy, showing adding of GO blocked part of the micropores and made the coating more compact and even.

Graphene oxide represents an intermediate byproduct arising during the production of graphene through the oxidation of graphite. It belongs to the class of two-dimensional materials like graphene[18]. GO is inherently hydrophilic, owing to the presence of oxygenated functional groups, including hydroxyl, epoxide, and carboxyl moieties, which significantly broaden its utility[19]. Research has already demonstrated that adding GO to the solution can significantly enhance the tribological properties of MAO coatings on magnesium and aluminum alloys[20,21]. However, there is limited research regarding the influence of GO concentration on MAO coatings for titanium alloys. In this article, an attempt has been made to explore influence of the amount of GO on MAO ceramic coating by changing the concentration of GO particles in the electrolyte during MAO process. The ceramic coatings were formed on Ti-6Al-4V titanium alloy by micro-arc oxidation with a DC power supply in the aluminate system electrolyte with and without GO. The phase constituent and microstructure of the ceramic coatings were analyzed by X-ray diffraction (XRD), and scanning electron microscopy (SEM). The friction reduction and wear resistance of the coatings prepared in electrolyte containing different concentration of graphene oxide were tested and analyzed. The effects of GO particle concentration on the thickness, hardness and roughness of the coatings were also discussed.

2. Experimental details

2.1. Material and MAO procedure

The Ti-6Al-4V alloy (5.5-6.75% Al, 3.5-4.5% V, 0-0.3% Fe, 0-0.2%O, and balance Ti) with a size of 50 × 20 × 1 mm were ground and polished with SiC abrasive paper to obtain an average roughness R_a ≈ 1.0 μm, and then washed in distilled water, ultrasonically degreased in alcohol prior to drying in cool air. A pulse power supply (MAO-WH30A-T) was used to perform MAO treatment at a constant voltage 350 V, frequency of 100 Hz, 10% duty cycle for 20 mins in a water-cooling bath with a stainless steel as cathode. The Ti-6Al-4V alloy sample was connected to the anode. The schematic diagram of the device is shown in Figure 1. Aqueous solutions of electrolytes were prepared using chemically pure $NaAlO_2$ and Na_3PO_4, and the concentration is 30 g/L $NaAlO_2$ and 5 g/L Na_3PO_4. The temperature was maintained between 17-19 ℃. A certain quantity of GO particles (particle size:10-40 μm) was added to the electrolyte to obtain different concentrations of 0,1,3,5,10 g/L with a magnetic stirrer operating to disperse GO particles. The ceramic coatings produced in the electrolyte containing 0, 1, 3, 5, 10 g/L GO were named as S0, S1, S3, S5, S10 respectively. Coated samples were flushed with water after the treatment and dried in warm air.

Preprints (www.preprints.org) | NOT PEER-REVIEWED | Posted: 20 October 2023 doi:10.20944/preprints202310.1334.v1

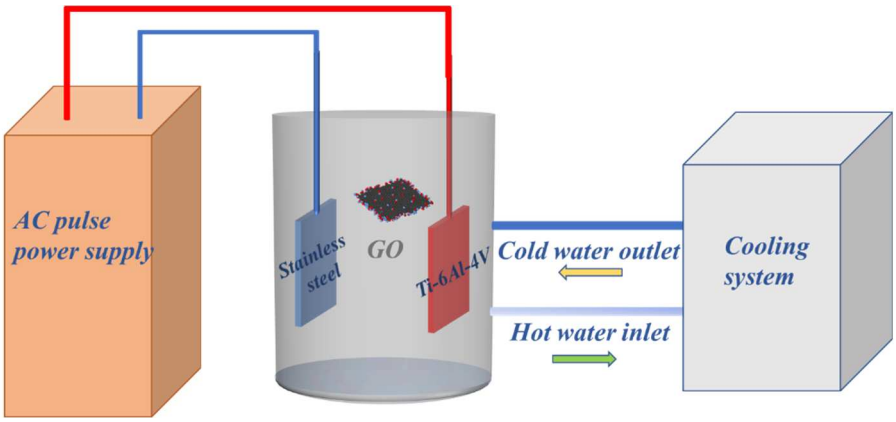

Figure 1. The schematic diagram of the experimental device.

2.2. Composition and microstructure analysis

The composition of coatings was explored by a grazing incidence X-ray diffractometer (Cu Kα radiation,) with the step size of 0.02° and a scan range of 20°-80°. The X-ray generator settings were 30 kV and 40 mA. A SEM was employed to observe the surface and cross-sectional microstructure. The thickness of the ceramic coatings was also observed and measured by a SEM. An energy dispersive spectrometer (EDS) attachment was used for qualitative element chemical analysis. The surface roughness of each coating was analyzed using a profilometer.

2.3. Tribological evaluation

The microhardness of the coatings was measured by a HVS-1000 Vickers hardness tester at a load of 1 kg. Ten different positions of each coated sample were tested. The tribological performance of MAO films were evaluated using a ball-on-disc tribology tester, which was carried out under a load of 3 N, 100 rpm and a diameter of 3 mm. The counter ball is made of SiC with a diameter of 6.35 mm, and the temperature was controlled to 20±1 ℃. After testing, the morphologies of the wear scars were observed by the scanning electron microscope, and the wear track diameter of the frictional counterparts was measured by an optical microscope.

3. Results and discussion

3.1. Phase composition

Figure 2 displayed the X-ray diffraction pattern of MAO ceramic coatings fabricated in electrolyte containing different amount of GO. It is clear that the predominant composition of all coatings is Al_2TiO_5, accompanied by a portion of γ-Al_2O_3 phase and minor quantities of low-valence titanium oxide. In addition, a small amount of rutile TiO_2 phase is also detected. Minor amounts of α-Al_2O_3 were detected in S1, S2, and S3, which were prepared in electrolyte with relatively low GO concentration. However, when the GO concentration reached 5 g/L and 10 g/L, α-Al_2O_3 was not detected in the coatings. The peak intensity of Al_2TiO_5 exhibits a decreasing trend with the increase in GO concentration. Furthermore, due to the thickness of the coatings, trace amounts of titanium were detected in all coatings.

 doi:10.20944/preprints202310.1334.v1

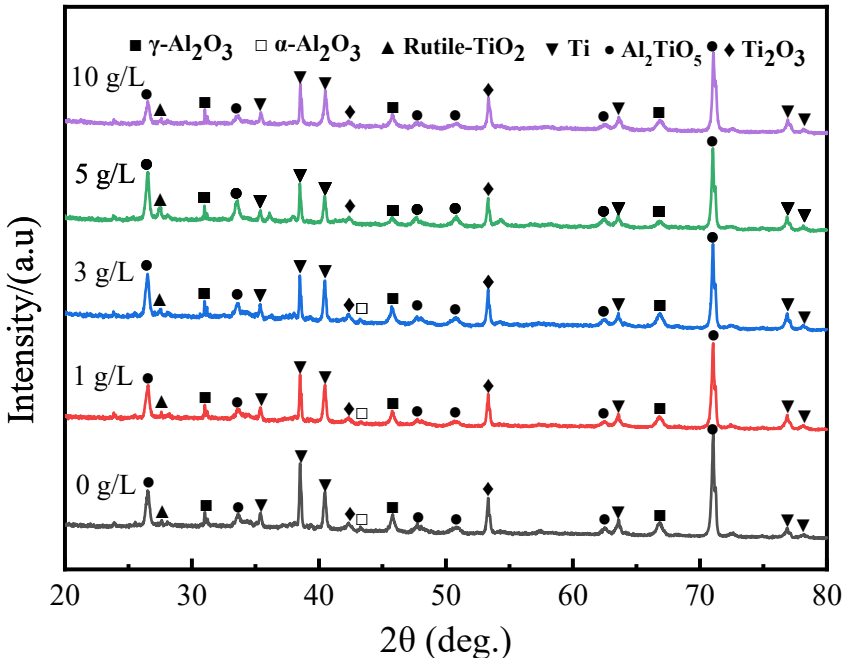

Figure 2. X-Ray diffraction patterns of MAO films produced in electrolytes with different concentrations of GO particles.

The relative content of the main elements Al, Ti, V and C on the surface of the coating was analyzed by EDS shown in Figure 3. The results indicate that with the increasing concentration of GO particles in the solution, there is an upward trend in the relative carbon content within the coatings Furthermore, increasing the GO concentration has minimal impact on the Al content, but leads to a decrease in Ti content within the coating. The particle concentration does not exhibit a significant impact on the vanadium element content within the coatings.

Observing the distribution map of Al elements, it can be noticed that the content of Al elements is nearly zero in certain regions. By combining this with SEM images, it becomes apparent that areas with low Al content correspond to the noticeable bumps (as shown by red circles) on the surface. This implies that the bump regions of the coating contain minimal aluminum oxides, and, in turn, suggests that the predominant constituents of these areas are titanium oxides.

Preprints (www.preprints.org) | NOT PEER-REVIEWED | Posted: 20 October 2023 doi:10.20944/preprints202310.1334.v1

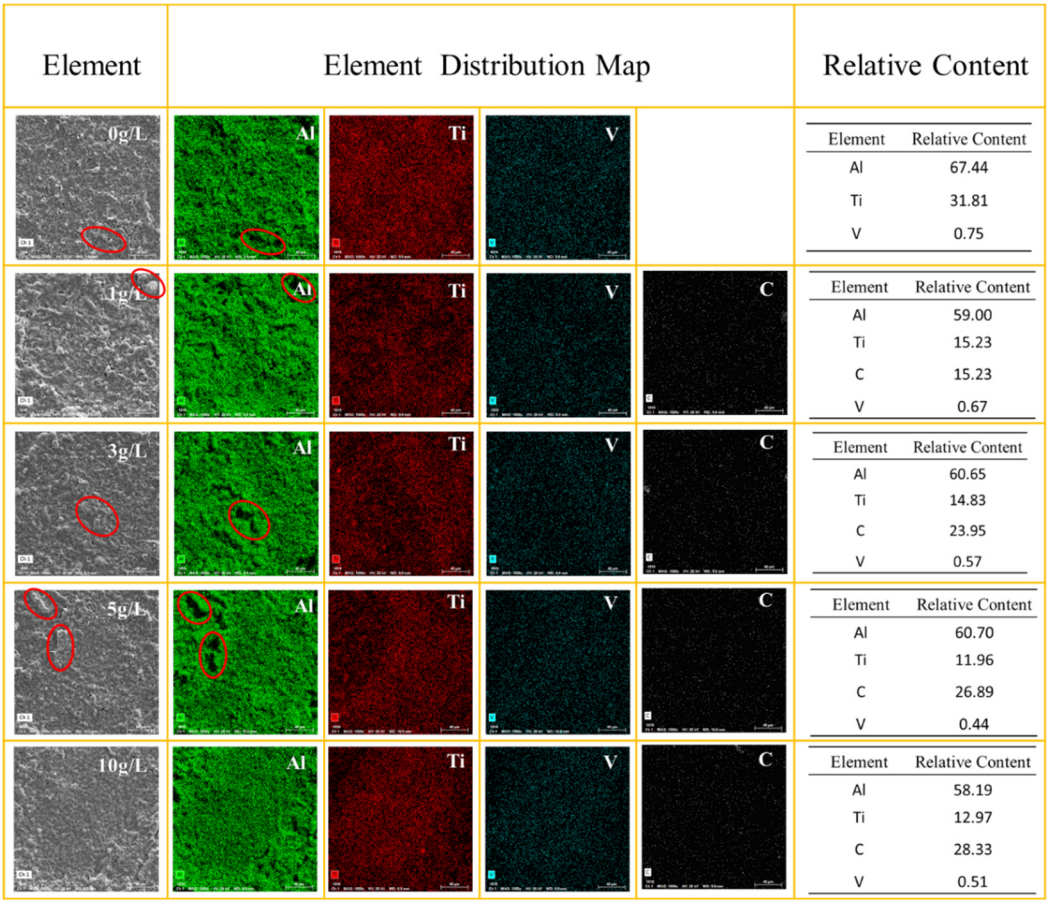

Figure 3. EDS analysis results on the surface of ceramic coatings.

3.2. Coating morphology

The surface morphologies of MAO coatings with different GO concentration are shown in Figure 4. From the magnified images, it can be observed that all MAO coatings exhibit a porous microstructure. The pores are typical features of MAO coatings which were mentioned in other papers[22]. These micro pores were possibly produced by eruption of melted material from inner part of the coating and emission of gas generated by the high-temperature of discharge[23,24]. From Figure 4, it can be observed that the coatings prepared in a solution containing no GO have slightly larger pore sizes than the other coatings, and the pore sizes of coatings containing different concentrations of GO do not show significant differences.

Furthermore, obvious cracks can be observed in Figure 4(a) and Figure 4(b) (as shown by yellow circles), the formation of cracks is due to the release of thermal stress generated during the film growth process[25,26]. The cracks become smaller and less noticeable on the surface of S3, S4 and S5, which indicates that the addition of GO can decrease thermal stress in the MAO treatment.

The introduction of GO particles into the MAO coatings significantly impacts the surface roughness and coating morphology. The surface of coating S2 and S3 is slightly smoother than that of the coating prepared in particle-free solution. It is clearly evident that the increase in GO concentration results in a smoother and more uniform surface of the coating. However, when the GO concentration reaches 10 g/L, the coating surface exhibits a laminar structure, which is completely different from the other four coatings. This implies relatively weak bonding strength between the layers. The reason is that excessive amount of GO got involved in the coating generation process, which weakened the cohesive strength between layers.

Preprints (www.preprints.org) | NOT PEER-REVIEWED | Posted: 20 October 2023 doi:10.20944/preprints202310.1334.v1

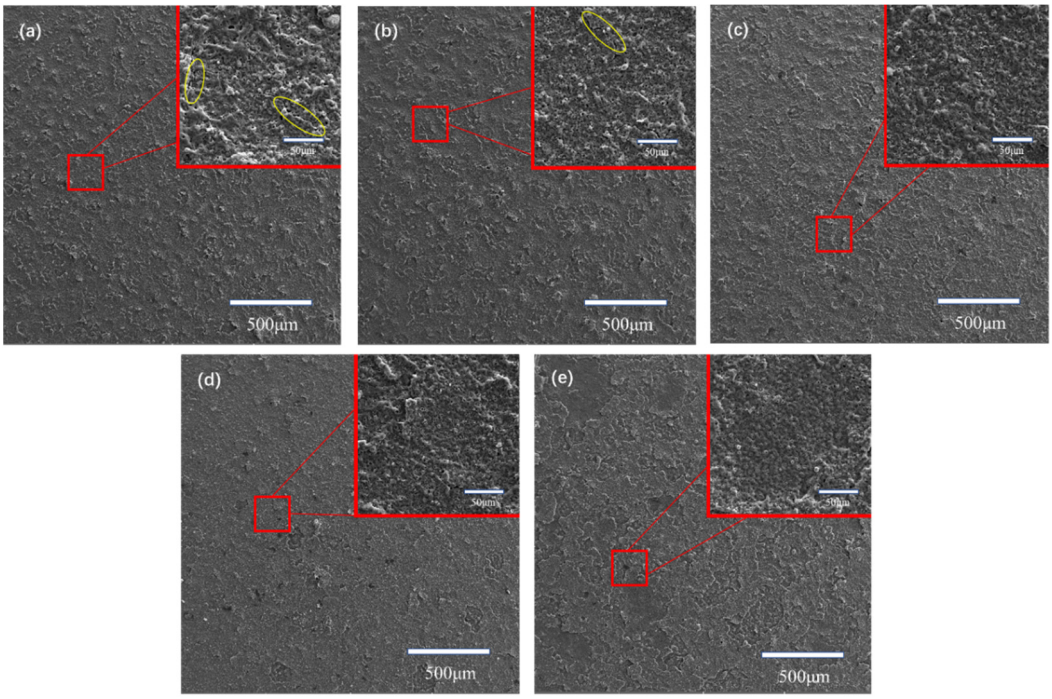

Figure 4. Surface morphology and microstructure of the MAO coatings by SEM: (a) S1; (b) S2; (c) S3; (d) S4; (e) S5.

Figure 5 illustrates the cross-sectional microstructure of the ceramic coatings that were generated in the electrolytes with different concentrations of GO particles. As shown in Figure 5, all coatings exhibited relatively uniform thickness. The addition of GO particles to the electrolyte had a significant effect on the thickness. It can be clearly seen that the coatings become thicker with the increase of GO concentration. As the GO concentration reaches 10 g/L, the thickness rises above 21 μm, which is twice that of the coating prepared in GO-free electrolyte. Several cavities can be clearly seen within the thickness of coating S1, whereas no significant pores were observed in the cross-sectional image of coating prepared in the GO-free electrolyte. This indicates that the addition of GO can reduce the porosity of the coating, thereby increasing its compactness.

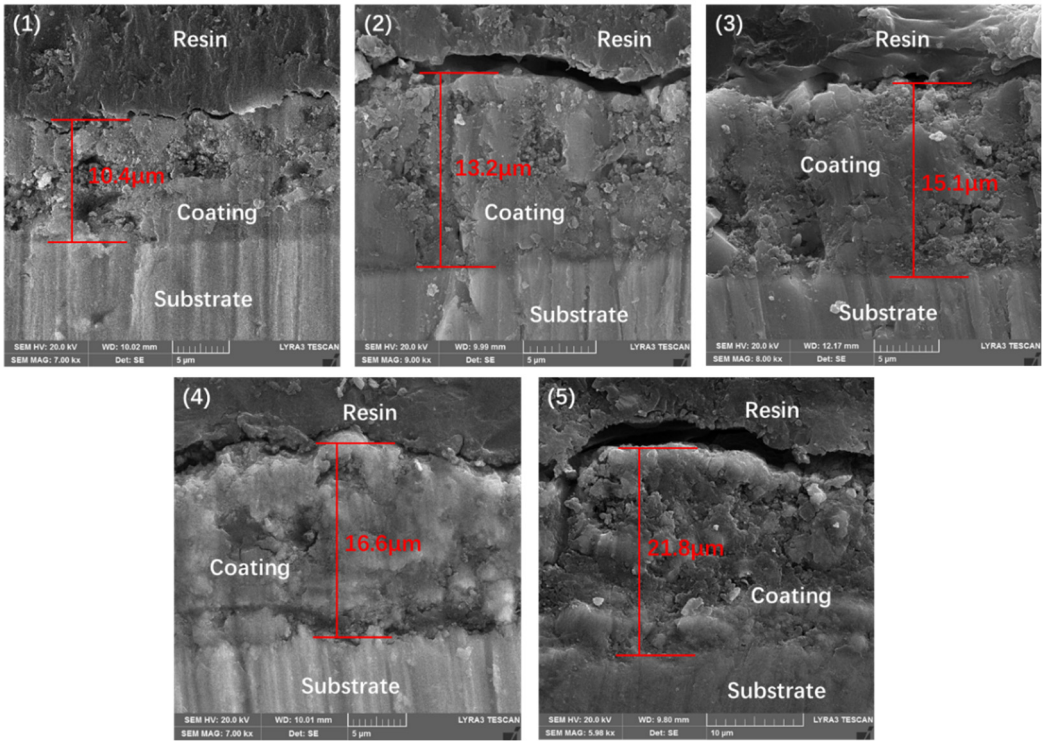

Preprints (www.preprints.org) | NOT PEER-REVIEWED | Posted: 20 October 2023 doi:10.20944/preprints202310.1334.v1

Figure 5. Cross-section microstructure of MAO coatings: (a) S1; (b) S2; (c) S3; (d) S4; (e) S5.

Figure 6 illustrates the surface roughness and hardness of MAO coatings prepared in electrolyte containing different concentrations of GO particles. The microhardness of the MAO coatings was measured by an HV-1000Z hardness tester at a load of 9.8 N applied to a Vickers indenter with a holding time 10 s. Coating S1 exhibits higher hardness compared to the other coatings, and furthermore, with the increasing concentration of GO, the hardness of the coatings shows a decreasing trend. The trend in hardness variations illustrating that the incorporation of GO leads to a decrease in coating hardness, and this decrease is positively correlated with the GO content. With the increase in GO concentration, more particles enter the coating, disrupting continuity of the coating, thereby leading to a decrease in hardness. The roughness of coatings S1, S2, and S3 is quite similar, indicating that there is minimal impact on roughness when the particle content is relatively low. This aligns with the observations by SEM analysis in Figure 4. The surface roughness of S4 and S5 is nearly identical, indicating that the reduction in coating surface roughness occurs only when the GO concentration surpasses a certain threshold.

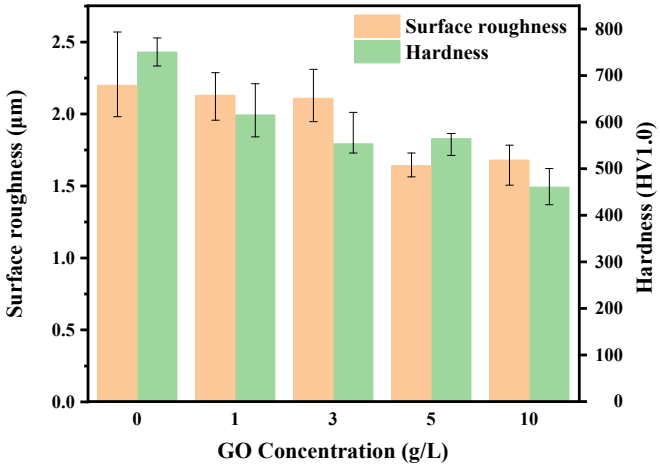

Figure 6. Surface roughness and hardness of MAO coatings with different concentrations of GO.

3.3. Tribological performance

Figure 7 shows the evolution of friction coefficient with sliding time under dry sliding condition for coatings prepared in electrolyte with different GO concentration. All coatings reached a relatively stable level of friction coefficient within five minutes. During the friction process, both the coating and the counterpart ball were continuously worn, resulting in an increasing contact area between them. This led to a gradual rise in the friction coefficient for all coatings over time. The friction coefficients of coating S1, S2, and S3 are all lower and more stable than that of the particle-free coating. As the GO concentration increased from 1 g/L to 5 g/L, the stable friction coefficients show a decreasing trend. However, when the GO concentration reached 10 g/L, the friction coefficient become higher than that of the particle-free coating. The decrease in the friction coefficient with an increase in particle concentration can be attributed to the GO nano-sheet acting as solid lubricants during the friction process. The increase in the friction coefficient of S5 can be attributed to excessively high concentrations causing a reduction in coating hardness. This results in wider wear tracks than those observed in other coatings, which implies a larger contact area during the friction process, subsequently leading to the higher friction coefficient.

Preprints (www.preprints.org) | NOT PEER-REVIEWED | Posted: 20 October 2023 doi:10.20944/preprints202310.1334.v1

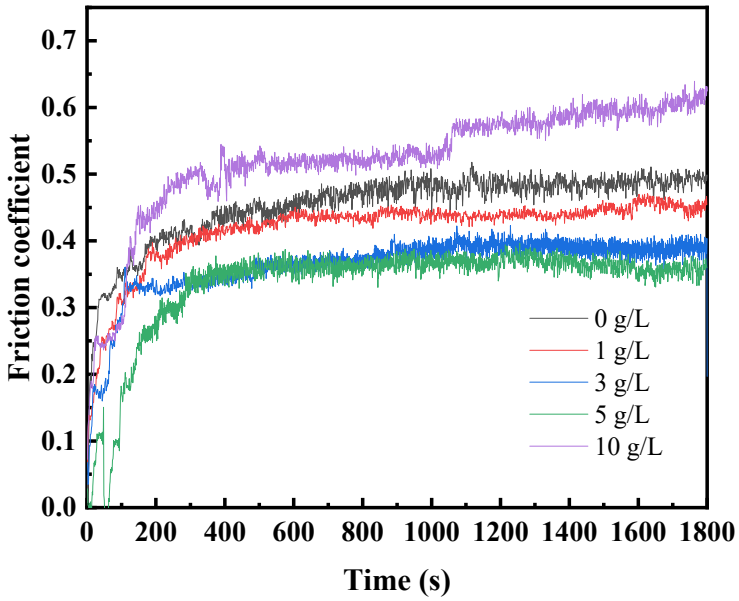

Figure 7. Friction coefficient of MAO coatings prepared with different concentrations of GO.

Scanning electron micrographs of the wear tracks generated on MAO coatings are exhibited in Figure 8. The coatings fabricated without the presence of GO in the solution exhibit the narrowest wear scar width. As the concentration of GO increases, the wear scar width become larger. The wear mechanism of MAO coatings can be easily obtained according to the scanning electron micrographs of the wear track. It can be clearly observed that plastic deformations occurred on central area of the wear scar on S1 coating, whereas, in contrast, the GO-composite coatings do not show distinct adhesive damage, which reveals the heavy ploughing because of abrasive wear. As illustrated in Figure 6, an increase in GO concentration correlates with a decrease in the hardness of the coating. Coatings with lower hardness are more susceptible to wear during the friction process, resulting in wider wear scars[27]. On the other hand, GO sheets act as lubricants during friction process, thereby reducing adhesive damage in the friction process and lowering the friction coefficient[28].

To further validate the impact of particle addition on the wear resistance of the coatings, the variations in wear scar diameter on the counterpart ball against different coatings were studied and shown in Figure 9. The results indicate that the changes in the diameter of the counter-material wear scars follow a similar pattern to the variations in coating wear scar width. With the increasing concentration of GO, the decrease in coating hardness results in reduced wear resistance, consequently leading to wider wear scars.

Preprints (www.preprints.org) | NOT PEER-REVIEWED | Posted: 20 October 2023 doi:10.20944/preprints202310.1334.v1

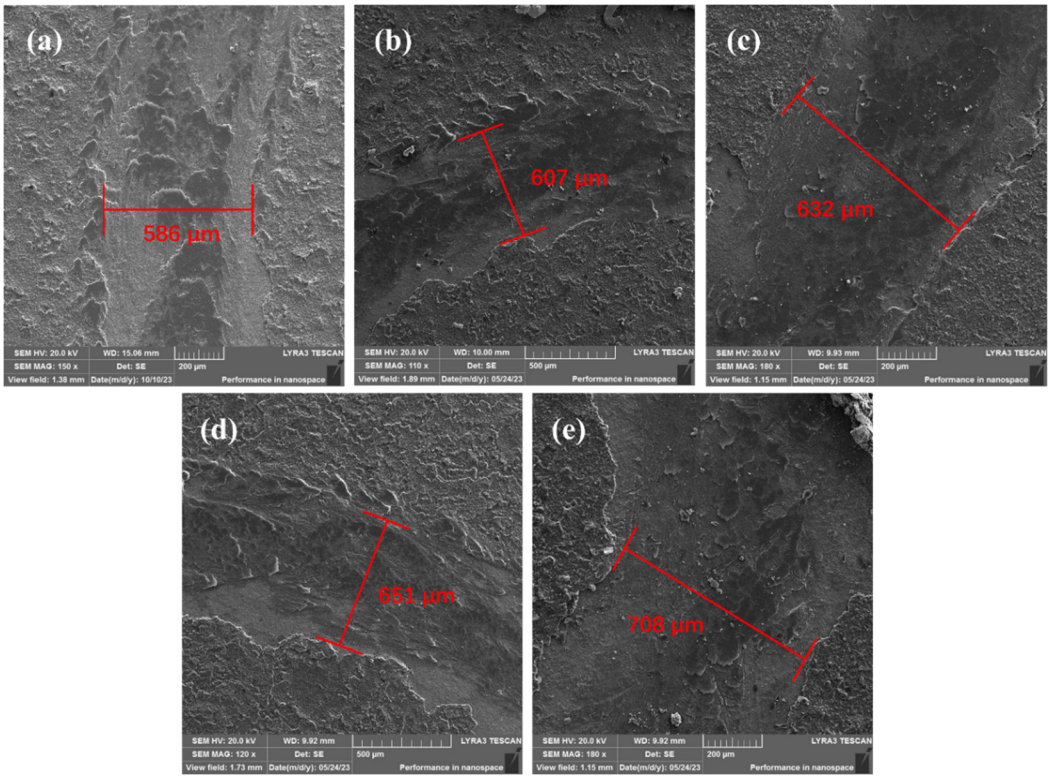

Figure 8. The wear tracks of the MAO coatings.

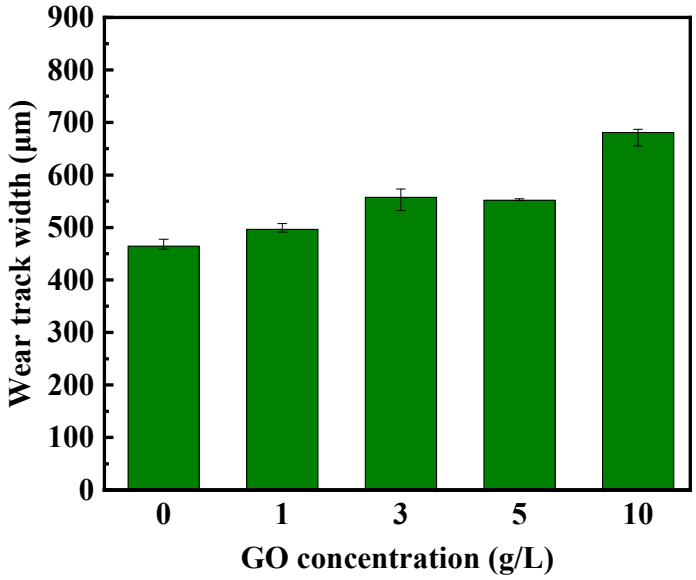

Figure 9. Wear track width of the counterpart.

To investigate the influence of GO concentration on the tribological performance of the coatings, the wear track depth profiles of the respective specimens were also measured and shown in Figure 10. The profile images of the wear scars on the coatings clearly reveal the variations in wear scar depth with changing GO concentrations. The coating without GO exhibits the shallowest wear scar. As the concentration increases, both the depth and width of the wear scar slightly increase, consistent with the SEM results. The wear track depth and width of S3 and S4 show no significant difference, as their hardness is almost the same in Figure 6. When the GO concentration reaches 10 g/L, the wear scar depth is approximately twice that of S1. The observed differences in wear track depth among the various coatings demonstrate a strong correlation with their respective hardness. With increasing GO

 doi:10.20944/preprints202310.1334.v1

concentration, the coating's hardness decreases, resulting in deeper wear scars during the friction process.

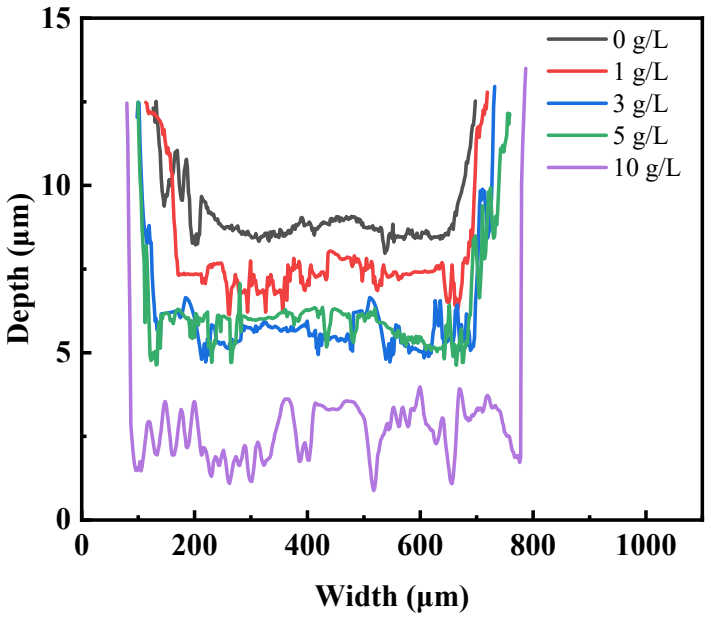

Figure 10. Depth profiles of the wear tracks.

4. Conclusions

GO particles were effectively incorporated into MAO coatings on the Ti-6Al-4V alloy surface. The composite coating consisted mainly of Al_2TiO_5, γ-Al_2O_3, with minor quantities of low-valence titanium oxide. Particle concentration had little impact on the coating composition. The addition of GO led to a smoother coating surface, with increased smoothness as particle concentration rose. However, at a 10 g/L concentration, excessive particles in the coating disrupted layer cohesion, resulting in a laminar structure on the coating surface.

The incorporation of GO reduced pore size and minimized surface microcracks, resulting in a denser coating structure. Coating hardness decreased with increasing particle concentration due to particle-induced structural disruption. Additionally, coating thickness significantly increased with rising concentration.

Incorporating GO reduced the friction coefficient, with the 5 g/L concentration coating demonstrating optimal anti-friction properties. However, coating hardness and wear resistance were inferior to GO-free coatings. Both wear scar width and depth increased with higher particle content due to the introduced GO disrupting coating structure and reducing cohesion. The addition of GO mitigated adhesive damage during friction, shifting the wear mechanism from adhesive to abrasive.

Author Contributions: Conceptualization, Q.H.; methodology, Q.D.; writing—original draft preparation, Q.H.; investigation, G.W.; formal analysis, X.L.; visualization, Y.R.; writing—review and editing, G.Z. All authors have read and agreed to the published version of the manuscript.

Funding: This project was financially supported by the NSFC (52075247, U2037603) and the Priority Academic Program Development of Jiangsu Higher Education Institutions (PAPD).

Institutional Review Board Statement: Not applicable.

Informed Consent Statement: Not applicable.

Data Availability Statement: The datasets used and/or analyzed during the current study are available from the corresponding author upon reasonable request.

Conflicts of Interest: The authors declare that they have no conflict of interest related to this work.

References

1. Yerokhin, A.L.; Nie, X.; Leyland, A.; Matthews, A. Characterisation of oxide films produced by plasma electrolytic oxidation of a Ti–6Al–4V alloy. *Surf. Coat. Technol.* **2000**, *130*, 195-206, https://doi.org/10.1016/S0257-8972(00)00719-2.
2. Wheeler, J.M.; Collier, C.A.; Paillard, J.M.; Curran, J.A. Evaluation of micromechanical behaviour of plasma electrolytic oxidation (PEO) coatings on Ti–6Al–4V. *Surf. Coat. Technol.* **2010**, *204*, 3399-3409, doi:10.1016/j.surfcoat.2010.04.006.
3. Zhai, D.; Feng, K.; Yue, H. Growth Kinetics of Microarc Oxidation TiO2 Ceramic Film on Ti6Al4V Alloy in Tetraborate Electrolyte. *Metallurgical and Materials Transactions A* **2019**, *50*, 2507-2518, doi:10.1007/s11661-019-05185-1.
4. Li, Q.; Yang, W.; Liu, C.; Wang, D.; Liang, J. Correlations between the growth mechanism and properties of micro-arc oxidation coatings on titanium alloy: Effects of electrolytes. *Surf. Coat. Technol.* **2017**, *316*, 162-170, doi:10.1016/j.surfcoat.2017.03.021.
5. Rakoch, A.G.; Gladkova, A.A.; Linn, Z.; Strekalina, D.M. The evidence of cathodic micro-discharges during plasma electrolytic oxidation of light metallic alloys and micro-discharge intensity depending on pH of the electrolyte. *Surf. Coat. Technol.* **2015**, *269*, 138-144, doi:10.1016/j.surfcoat.2015.02.026.
6. Habazaki, H.; Tsunekawa, S.; Tsuji, E.; Nakayama, T. Formation and characterization of wear-resistant PEO coatings formed on β-titanium alloy at different electrolyte temperatures. *Appl. Surf. Sci.* **2012**, *259*, 711-718, doi:10.1016/j.apsusc.2012.07.104.
7. Yin, X.; Wang, Y.; Liu, B.; Luo, X.B. Effects of the grain boundary on phase structure and surface morphology of TiO2 films prepared by MAO technology. *Surf. Interface Anal.* **2012**, *44*, 276-281, doi:https://doi.org/10.1002/sia.3792.
8. Aliasghari, S.; Skeldon, P.; Thompson, G.E. Plasma electrolytic oxidation of titanium in a phosphate/silicate electrolyte and tribological performance of the coatings. *Appl. Surf. Sci.* **2014**, *316*, 463-476, doi:https://doi.org/10.1016/j.apsusc.2014.08.037.
9. Matykina, E.; Berkani, A.; Skeldon, P.; Thompson, G.E. Real-time imaging of coating growth during plasma electrolytic oxidation of titanium. *Electrochim. Acta* **2007**, *53*, 1987-1994, doi:10.1016/j.electacta.2007.08.074.
10. Wang, Y.; Jiang, B.; Lei, T.; Guo, L. Dependence of growth features of microarc oxidation coatings of titanium alloy on control modes of alternate pulse. *Mater. Lett.* **2004**, *58*, 1907-1911, doi:10.1016/j.matlet.2003.11.026.
11. Sobolev, A.; Kossenko, A.; Borodianskiy, K. Study of the Effect of Current Pulse Frequency on Ti-6Al-4V Alloy Coating Formation by Micro Arc Oxidation. *Materials* **2019**, *12*, doi:10.3390/ma12233983.
12. Venkateswarlu, K.; Suresh, S.; Nagumothu, R.; Sreekanth, D.; Sandhyarani, M. Role of Electric Pulse Duty and Frequency on Properties of Micro-Arc Oxidized Titania Films Developed on Ti-6Al-4V. *Mater. Sci. Forum* **2013**, *765*, 688-692, doi:10.4028/www.scientific.net/MSF.765.688.
13. Wang, J.-H.; Wang, J.; Lu, Y.; Du, M.-H.; Han, F.-Z. Effects of single pulse energy on the properties of ceramic coating prepared by micro-arc oxidation on Ti alloy. *Appl. Surf. Sci.* **2015**, *324*, 405-413, doi:https://doi.org/10.1016/j.apsusc.2014.10.145.
14. Martin, J.; Melhem, A.; Shchedrina, I.; Duchanoy, T.; Nominé, A.; Henrion, G.; Czerwiec, T.; Belmonte, T. Effects of electrical parameters on plasma electrolytic oxidation of aluminium. *Surf. Coat. Technol.* **2013**, *221*, 70-76, doi:10.1016/j.surfcoat.2013.01.029.
15. Chang, F.-C.; Wang, C.-J.; Lee, J.-W.; Lou, B.-S. Microstructure and mechanical properties evaluation of molybdenum disulfide-titania nanocomposite coatings grown by plasma electrolytic oxidation. *Surf. Coat. Technol.* **2016**, *303*, 68-77, doi:10.1016/j.surfcoat.2016.03.078.
16. Liu, W.; Blawert, C.; Zheludkevich, M.L.; Lin, Y.; Talha, M.; Shi, Y.; Chen, L. Effects of graphene nanosheets on the ceramic coatings formed on Ti6Al4V alloy drill pipe by plasma electrolytic oxidation. *J. Alloys Compd.* **2019**, *789*, 996-1007, doi:10.1016/j.jallcom.2019.03.060.
17. Zhang, Y.; Chen, F.; Zhang, Y.; Du, C. Influence of graphene oxide additive on the tribological and electrochemical corrosion properties of a PEO coating prepared on AZ31 magnesium alloy. *Tribology International* **2020**, *146*, 106135, doi:https://doi.org/10.1016/j.triboint.2019.106135.
18. Grigoriev, S.; Peretyagin, N.; Apelfeld, A.; Smirnov, A.; Morozov, A.; Torskaya, E.; Volosova, M.; Yanushevich, O.; Yarygin, N.; Krikheli, N.; et al. Investigation of Tribological Characteristics of PEO Coatings Formed on Ti6Al4V Titanium Alloy in Electrolytes with Graphene Oxide Additives. *Materials* **2023**, *16*, doi:10.3390/ma16113928.
19. Shang, W.; Wu, F.; Wang, Y.; Rabiei Baboukani, A.; Wen, Y.; Jiang, J. Corrosion Resistance of Micro-Arc Oxidation/Graphene Oxide Composite Coatings on Magnesium Alloys. *ACS Omega* **2020**, *5*, 7262-7270, doi:10.1021/acsomega.9b04060.
20. Yang, W.; Xu, D.P.; Wang, J.L.; Jiang, B.L. Preparation of MAO coatings doped with graphene oxide. *Surf. Eng.* **2017**, *33*, 739-743, doi:10.1080/02670844.2016.1188498.

21. Zhang, Y.; Chen, F.; Zhang, Y.; Liu, Z.; Wang, X.; Du, C. Influence of graphene oxide on the antiwear and antifriction performance of MAO coating fabricated on MgLi alloy. *Surf. Coat. Technol.* **2019**, *364*, 144-156, doi:https://doi.org/10.1016/j.surfcoat.2019.01.103.
22. Chen, X.; Hu, J.; Zhang, D.; Ren, P.; Liao, D.; Cai, L. Study on corrosion resistance of TC4 titanium alloy micro-arc oxidation/(PTFE + graphite) composite coating. *Int. J. Appl. Ceram. Technol.* **2021**, *19*, 397-408, doi:10.1111/ijac.13891.
23. Ma, K.-J.; Al Bosta, M.M.S.; Wu, W.-T. Preparation of self-lubricating composite coatings through a micro-arc plasma oxidation with graphite in electrolyte solution. *Surf. Coat. Technol.* **2014**, *259*, 318-324, doi:10.1016/j.surfcoat.2014.03.004.
24. Li, H.; Sun, Y.; Zhang, J. Effect of ZrO2 particle on the performance of micro-arc oxidation coatings on Ti6Al4V. *Appl. Surf. Sci.* **2015**, *342*, 183-190, doi:10.1016/j.apsusc.2015.03.051.
25. Xue, W.; Wang, C.; Chen, R.; Deng, Z. Structure and properties characterization of ceramic coatings produced on Ti–6Al–4V alloy by microarc oxidation in aluminate solution. *Mater. Lett.* **2002**, *52*, 435-441, doi:https://doi.org/10.1016/S0167-577X(01)00440-2.
26. Shokouhfar, M.; Allahkaram, S.R. Formation mechanism and surface characterization of ceramic composite coatings on pure titanium prepared by micro-arc oxidation in electrolytes containing nanoparticles. *Surf. Coat. Technol.* **2016**, *291*, 396-405, doi:https://doi.org/10.1016/j.surfcoat.2016.03.013.
27. Martini, C.; Ceschini, L.; Tarterini, F.; Paillard, J.; Curran, J. PEO layers obtained from mixed aluminate–phosphate baths on Ti–6Al–4V: Dry sliding behaviour and influence of a PTFE topcoat. *Wear* **2010**, *269*, 747-756, doi:10.1016/j.wear.2010.07.011.
28. Wu, G.; Yin, Y.; Zhang, S.; Wang, Y.; Xiang, Y.; Li, L.; Yao, J. Effect of laser texturing on the antiwear properties of micro-arc oxidation coating formed on Ti-6Al-4V. *Surf. Coat. Technol.* **2023**, *453*, doi:10.1016/j.surfcoat.2022.129114.